

Discovery of hard X-ray features around the hotspots of Cygnus A

M. Bałucińska-Church^{1,2}, M. Ostrowski^{2,3}, L. Stawarz² and M. J. Church^{1,2} *

¹*School of Physics and Astronomy, University of Birmingham, Birmingham B15 2TT, UK*

²*Obserwatorium Astronomiczne, Uniwersytet Jagielloński, ul. Orla 171, 30-244 Kraków, Poland*

³*Institut für Theoretische Physik IV, Ruhr-Universität Bochum, D-44780 Bochum, Germany*

Received June 22nd, 2004. Accepted November 8th, 2004.

ABSTRACT

We present results of analysis of a *Chandra* observation of Cygnus A in which the X-ray hotspots at the ends of the jets are mapped in detail. A hardness map reveals previously unknown structure in the form of outer and inner hard arcs around the hotspots, with hardness significantly enhanced compared with the hotspot central regions. The outer hard arcs may constitute the first detection of the bow shock; the inner hard arcs may reveal where the jets impact on the hotspots. We argue that these features cannot result from electrons radiating by the synchrotron self-Compton process. Instead we consider two possible sources of the hard emission: the outer arcs may be due to thermal radiation of hot intracluster gas compressed at the bow shock. Alternatively, both outer and inner arcs may be due to synchrotron radiation of electrons accelerated in turbulent regions highly perturbed by shocks and shear flows. Comparison of measured hardness ratios with simulations of the hardness ratios resulting from these processes show that it is more difficult to explain the observations with a thermal model. Although we cannot rule out a thermal model, we argue in favour of the non-thermal explanation. The hard regions in the secondary hotspots suggest that jet activity is still powering these hotspots.

Key words: galaxies: active—galaxies: individual (Cygnus A)—X-rays: individual (Cygnus A)

1 INTRODUCTION

In the brightest radio galaxies, hotspots at the ends of the radio jets are often found which radiate from radio to X-rays. Blandford & Rees (1974) and Scheuer (1974) proposed that these are formed where the jet interacts with the ambient medium and decelerates abruptly forming a double shock structure. The forward shock (the ‘bow shock’) compresses and heats the intergalactic medium. The reverse shock (the ‘Mach shock’) propagates within the jet, converting the jet bulk kinetic energy into cosmic ray particles and magnetic field energy. The interaction of the jet with the compressed ambient gas turns the shocked jet matter backwards to expand into the radio lobes. The observed hotspots are generally thought to be located downstream of the reverse shock, but whether they extend to the bow shock is not clear.

Radio observations of the hotspots show highly polarized broadband emission of power law spectral form, without doubt synchrotron in origin. This emission extends in some

cases to the optical band (Meisenheimer et al. 1989). The observations often reveal a complex radio morphology in the jet terminal regions, with the presence of multiple hotspots (e.g. Hardcastle et al. 1998). Several explanations have been proposed for these, including formation by precession of the jets on relatively short timescales (Scheuer 1982), or the deflection of the jets at the terminal point due to extended oblique shocks at the jet head (Williams & Gull 1985). The time-dependent nature of the hotspots may also be related to modulation of the kinetic power of the jet (Leahy & Perley 1995; see also Stawarz et al. 2004).

As the synchrotron lifetime of the radio and optical emitting electrons (in the equipartition magnetic field) is typically much shorter than the light-crossing time between the nucleus and the hotspot region (Hargrave & Ryle 1974, Meisenheimer et al. 1989, Brunetti et al. 2003), it is thought that there must be *in situ* particle acceleration within the hotspots. Heavens & Meisenheimer (1987) proposed a particular model in which such an acceleration takes place at the Mach shock, providing a power law population of ultrarelativistic electrons which cool radiatively by the synchrotron and inverse-Compton processes in a localized downstream

* E-mail: mbc@star.sr.bham.ac.uk, mio@oa.uj.edu.pl, stawarz@oa.uj.edu.pl, mjc@star.sr.bham.ac.uk

region where the magnetic field strength is high (the ‘continuous injection’ model). In most cases, the radio-to-infrared spectra of the hotspot emission can be explained by this model (Meisenheimer et al. 1989). Apart from this localized acceleration, some infrared and optical observations provide evidence for an acceleration process distributed around the hotspots. Diffuse infrared emission extending a few kpc beyond the hotspot was detected in 3C 445 (Prieto, Brunetti & Mack 2002), Pictor A (Röser & Meisenheimer 1987) and in 3C 273 (Meisenheimer 2003). It was suggested that the appropriate mechanism consists of stochastic acceleration processes at strong turbulence surrounding the hotspot (Meisenheimer, Yates & Röser 1997, Prieto et al. 2002).

X-ray emission from several radio hotspots was detected using *ROSAT*. More recently, the spatial resolution and high sensitivity of *Chandra* has allowed the study of a larger number of hotspots in powerful radio sources (Hardcastle et al. 2004). For some of these hotspots, the X-ray emission is consistent with production by the synchrotron self-Compton process (SSC). This allows estimation of the magnetic field strength often yielding values close to the equipartition value. However, X-ray hotspot emission in several sources cannot be explained in terms of a SSC model (Hardcastle et al. 2004), suggesting that the keV photons most probably have synchrotron origin.

In Cyg A (Fig. 1), the jets form primary hotspots B and E and secondary hotspots A and D in the Western and Eastern lobes, respectively, as designated by Hargrave & Ryle (1974). The radio hotspots A and D are highly polarized, roughly spherically shaped, with radius ≈ 2 kpc and bolometric luminosity $L_{\text{syn}} \approx 4 \times 10^{44}$ erg s $^{-1}$ (Carilli & Barthel 1996). Carilli et al. (1991, 1999) and Meisenheimer et al. (1997) showed that the synchrotron emission of hotspots A and D extending to at least 10^{12} Hz, with a high-frequency cut-off at $\sim 10^{13}$ Hz implied by the optical upper limit, is consistent with the ‘continuous injection’ model. The breaks in the radio spectra allow physical parameters to be constrained for these two hotspots, with the magnetic field strength derived being consistent with the equipartition value $B_{\text{eq}} \approx 3 \times 10^{-4}$ G, the related minimum hotspot pressure $p_{\text{eq}} \approx 3 \times 10^{-9}$ dyn cm $^{-2}$, and the downstream velocity of the radiating plasma $\beta_{\text{out}} \approx 0.05 - 0.1$.

The hotspots A and D were detected in X-rays using *ROSAT* (Harris, Carilli & Perley 1994), who showed that the X-ray emission was non-thermal, as a thermal model required a particle number density far above the upper limit allowed by the lack of internal radio depolarization, $n_{\text{th}} < 4 \times 10^{-4}$ cm $^{-3}$ (Dreher, Carilli & Perley 1987). Spectral analysis of the hotspots in the present *Chandra* observation allowed Wilson, Young & Shopbell (2000) to obtain a X-ray power law energy index $\alpha_X \approx 0.8$, and a X-ray hotspot luminosity, $L_X \approx 10^{42}$ erg s $^{-1}$. These can be explained as SSC emission for a magnetic field strength $B \sim 1.5 \times 10^{-4}$ G (Harris et al. 1994; Wilson, Young & Shopbell 2000), a value close to B_{eq} . Because of this, the hotspots A and D in Cygnus A are generally accepted as standard examples of astrophysical objects justifying the equipartition hypothesis (cf. Kino & Takahara 2004). In the present paper, we find previously-unknown hardness variations across the X-ray hotspots of Cygnus A implying significant substructure.

Figure 1. *Chandra* ACIS X-ray intensity image of Cygnus A in the energy band 0.3 – 12 keV, with 5 GHz radio contours superimposed (kindly provided by C. L. Carilli).

2 OBSERVATIONS AND ANALYSIS

We have analysed the observation of Cygnus A made with *Chandra* on May 21, 2000 UT 03:13:30 – 13:25:55, with a total usable exposure of ~ 34000 s. Data analysis was carried out using CIAO version 3.0.2 and the latest calibration data (Feb 2, 2004). Events files were produced which had been checked for bad pixels and high background, and corrections made for charge transfer inefficiency and gain variations in the image. X-ray images were produced using DMCPY of size 350×287 0.49" pixel, sufficient to contain all of Cyg A. The intensity images were not converted to flux images as this process makes assumptions about the spectrum, and the intensity image in the band 0.3–8.0 keV image with 5 GHz radio contours superimposed is shown in Fig. 1.

We attempted to carry out spectral fitting by dividing each hotspot into an outer region (away from the nucleus) and an inner region. However, the total count in each of these regions was 140 which does not allow sensible spectral fitting, not allowing discrimination between thermal and non-thermal models. Previous analysis of this observation (Wilson et al. 2000) used the whole of hotspots A and D.

Because of the difficulty of spectral fitting with smaller regions, we used X-ray hardness ratios to constrain spectral changes within the source. We obtained images using DMCPY in two energy bands: 2.0–8.0 keV and 0.3–2.0 keV, which were divided to give a hardness map. As there is a wide range of intensity at the hotspots with pixels in outer regions having large Poisson fluctuations, it is necessary to use either adaptive smoothing or adaptive binning (Sanders & Fabian 2001). Firstly, we smoothed adaptively in each energy band using CSMOOTH. The hardness map displays significant changes across the whole image of Cyg A: in the central plane perpendicular to the jets, along the jets and in the hotspots. In this Letter we discuss the hardness variations in the hotspots. Care has to be taken in using adaptive smoothing because the Gaussian width σ used in smoothing the high energy band with less counts will be larger than in the low band, and this *might* lead to a hard annulus around a hotspot as an artifact. To avoid this possibility we carried out the smoothing in both bands using σ values at every position in the image derived from the band 0.3–2.0 keV. The resulting hardness map for each hotspot is shown in Fig. 2, with X-ray intensity contours (0.3–8.0 keV) superimposed. Strong hardness variations are seen in each hotspot, and clearly the hardness ratio (HR) does not correlate with X-ray intensity. On the contrary, the peak of X-ray intensity is the least hard, with hard features around the outsides which, being extended, we term hard arcs. Spot A in particular shows the softer region extending along the axis of elongation of the intensity contours, approximately perpendicular to the direction of the jet. The HR values increase by a factor of two to three from the centres to the hard outer regions. A possible objection to adaptive smoothing is that it involves some redistribution of the counts. We also carried out adaptive binning of the data in the two energy bands to avoid this, which bins together several pixels in the outer

Figure 2. X-ray hardness with the intensity contours superimposed. Left panel: the counter jet hotspot D, right panel: the jet hotspots A and B. Hardness increases from blue to yellow. Image sizes are $19'' \times 15''$. The variation in hardness across the hotspots is seen.

hotspots to reduce Poisson fluctuations to a specified level (35 percent). There was general agreement with the results of adaptive smoothing, with the centres of the hotspots being less hard, and hard regions around the hotspots. Beyond this, the count statistics do not allow more precise definition of the hard region geometry. We noted a slight tendency for the hard regions to be moved radially outwards in adaptive smoothing probably related to the redistribution of counts. However, the adaptively smoothed images are better for display.

We used the adaptively binned images to obtain mean values of hardness since this is equivalent to using raw data. Average values of hardness were obtained from 4 rebinned pixels (14 primitive pixels) for spot A including the hard regions on both sides of the hotspot, giving $HR = 0.77 \pm 0.16$. The central region had $HR = 0.29 \pm 0.13$. Thus the change is highly significant. For spot D, the corresponding values are $HR = 0.79 \pm 0.16$ in 9 pixels and 0.33 ± 0.10 , and for spot B the values are 0.79 ± 0.16 and 0.32 ± 0.11 .

To assess the implications of the hardness changes, spectral data were simulated for a simple absorbed power law: AB*PL for a range of photon power law index Γ , and for an absorbed Mekeal model: AB*ME for a range of kT , using large normalizations to avoid Poisson fluctuations. Then the data were divided into the same two energy bands as in our analysis and the hardness ratio found. The column density was fixed at $0.3 \times 10^{22} \text{ atom cm}^{-2}$ from radio determinations near the hotspot (Dickey & Lockman 1990). The mean HR in the hard arcs (above), and at peak intensity in each hotspot are compared with the simulations (dashed curves) in Fig. 3. The X-ray intensity falls sharply with radial distance from the centre of each hotspot, continuing to decrease on the outside of each hotspot (away from the nucleus). We chose to determine the background at an outside radial position of $3.5''$, but this may still be an overestimate. Because of this uncertainty, in Fig. 3 we plot hardness values *before* background correction and show the probable maximum extent of the correction for the hard arc points as dotted lines. The correction would *increase* the change in hardness across each hotspot. At the peak of X-ray intensity, the effect of background subtraction is negligible.

The above HR values for the hard arcs intersect the power law curve at $\Gamma = 1.23 \pm 0.20$, 1.20 ± 0.20 and 1.20 ± 0.20 for spots A, D and B, and for the peak intensity at $\Gamma = 2.18 \pm 0.42$, 2.07 ± 0.30 and 2.10 ± 0.34 for the same three hotspots. Thus the change in power law index between the peak intensity and the hard arc is $\Delta\Gamma = 0.96 \pm 0.47$, 0.88 ± 0.36 and 0.91 ± 0.39 for hotspots A, D and B.

When compared with the Mekeal model, it can be seen that hardness ratios of 0.29, 0.33 and 0.32 can be *formally* explained by a kT of 2.85, 3.22 and 3.09 keV at the peak of X-ray intensity, although we know in this case that the emission is non-thermal. The hard arcs require $kT = 96$ (-84), 180 (-165) and 177 (-163) keV for spots A, D and B; at the upper limit of HR, there is no intersection with the curve.

3 ORIGIN OF THE HARD FEATURES

The hard arcs discovered in the present work cannot be explained in the framework of the SSC process. Carilli et al. (1991) argued that at the edges of the hotspots the shock-generated electron energy distribution would adopt the Jaffe-Perola or the Kardashev-Pacholczyk shape, i.e. a sharp cut-off or steep power law in the high energy range. Thus SSC X-ray emission would always be (at least a bit) softer at the outer edge of the hotspot than inside at the X-ray intensity peak, contrary to Fig. 2. Thus, we consider other possible mechanisms for producing the hard regions.

A natural source of hardening for the outer arcs, i.e. on the outsides of the hotspots, could be the thermal radiation of ambient intracluster gas compressed and heated by the bow shock. This shocked gas forms the sheath behind the bow shock in pressure equilibrium with the shocked jet plasma, for which the minimum pressure is $p_{eq} \approx 3 \times 10^{-9} \text{ dyn cm}^{-2}$ (Sect. 1). Ram pressure confinement of the hotspot implies that $\rho_g v_{sh}^2 = p_{eq}$, and hence that $\mathcal{M}_{sh} = (p_{eq}/\hat{\gamma}_g p_g)^{1/2}$, where ρ_g , p_g and $\hat{\gamma}_g$ are the density, the pressure and the ratio of specific heats of the unperturbed ambient gas ('g'). v_{sh} and \mathcal{M}_{sh} are the bow shock velocity and Mach number: $\mathcal{M}_{sh} \equiv v_{sh}/c_{s,g}$, where the sound speed of the unperturbed ambient gas is $c_{s,g} = (\hat{\gamma}_g p_g/\rho_g)^{1/2}$. For $\hat{\gamma}_g = 5/3$ and $p_g \approx 10^{-10} \text{ dyne cm}^{-2}$ (Smith et al. 2002) one gets $\mathcal{M}_{sh} \approx 5$ which is a lower limit as the *minimum* hotspot pressure was used. From the Mach number, we can estimate the temperature of the shock-heated gas ($kT_{g,+}$) and the compression ratio of the bow shock from the Rankine-Hugoniot conditions, giving $kT_{g,+} \approx 8.7 \times kT_g \approx 43.4 \text{ keV}$ and $n_{g,+} \approx 3.6 \times n_g \approx 0.036 \text{ cm}^{-3}$ for a temperature and density of the unperturbed intracluster gas of $kT_g \approx 5 \text{ keV}$ and $n_g \approx 10^{-2} \text{ cm}^{-3}$ (Smith et al. 2002; see also Harris et al. 1994). The hardness of the hard outer arcs in spots A and D (Fig. 2) correspond to $kT \sim 96$ and 180 keV in the simulated data with large errors, i.e. $kT > 10$ and 15 keV , respectively. Thus we cannot rule out thermal origin of the hard outer arcs. However, the plasma density at the inner hard regions probably close to the jet terminal shock is thought to be low so that thermal radiation cannot explain these.

A thermal origin of the outer arcs would be supported by observation of related structures in the Faraday rotation radio maps, because the compression behind the bow shock can cause some change in polarization of a fraction of the radio emission (Carilli, Perley & Dreher (1988). We evaluate the total Faraday rotation within the shocked thermal gas layer using the above shock and intracluster parameters, i.e. an electron density in the shocked sheath $n_{g,+} \approx 0.04 \text{ cm}^{-3}$ and a mean magnetic field $B_{g,+} \approx 20 \mu\text{G}$. The sheath thickness h is the hotspot size divided by $2\sqrt{5}$ (Carilli et al. 1988), i.e. $\approx 200 \text{ pc}$. As the sheath is curved, resembling the Earth's bow shock in the solar wind, the mean radio wave propagation length, l , through this layer will be a few times h , say 500 pc . For a wavelength $\lambda = 6 \text{ cm}$ and $B_{g,\parallel} \approx B_{g,+}/2$, with these units, the characteristic Faraday rotation angle $\Delta\Psi = 8.1 \times 10^{-3} \lambda^2 B_{g,\parallel} l n_{g,+}$ is $\Delta\Psi \approx 0.6 \text{ rad}$. Thus *variation* in the rotation angle across the region

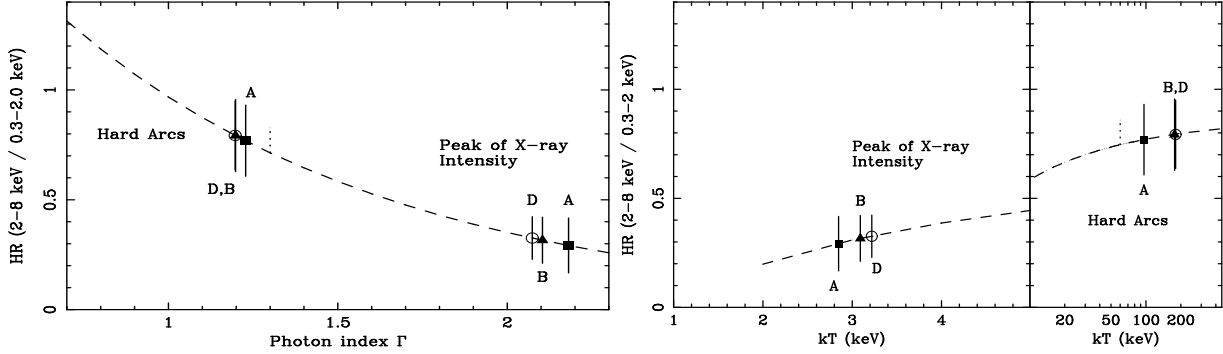


Figure 3. Comparison of measured enhancements of hardness in the hard arcs with simulations. Left panel: non-thermal model; right panel: thermal model. The dotted lines show the maximum correction due to background subtraction. In the thermal model, the point for hotspot A never intersects the dashed line, and is arbitrarily shown at 50 keV; the point for hotspot D intersects at 38 keV.

at $\lambda \lesssim 6$ cm will also be small, and so depolarization will be small.

Both inner and outer hard regions may be non-thermal in origin, but the extremely flat spectral index $\alpha_X \sim 0$ implied by $\Gamma \sim 1$ excludes inverse Compton radiation produced by the electrons responsible for the hotspot radio emission, as the radio spectral index in the hotspot regions is $\alpha_R \gtrsim 0.5$. Instead, we have to consider synchrotron emission of an additional, high-energy flat electron population $n_e(\gamma) \sim \gamma^{-1}$, where γ is the electron Lorentz factor. A natural possibility for the formation of such an additional electron component is turbulent particle acceleration within an extended region where the particle escape/advection timescale is much longer than the radiative timescale (Stawarz & Ostrowski 2002; Stawarz et al. 2004 and references therein). For the outer arcs, this could be near the contact discontinuity; for the inner arcs near the jet terminal shock. As suggested by numerical simulations, the hotspot downstream regions near the contact discontinuity between shocked jet fluid and shocked ambient gas can be indeed highly turbulent (Mizuta, Yamada & Takabe 2004 and deYoung 2002). The electrons in such regions are subject to repeated scattering by fast moving MHD waves and undergo diffusion in momentum space. This process may produce cosmic ray electrons with spectrum determined by the acceleration timescale, $t_{\text{acc}}(\gamma)$, the radiative loss timescale, $t_{\text{rad}}(\gamma)$, and the timescale for particle escape from the acceleration region, $t_{\text{adv}}(\gamma)$. For $t_{\text{rad}} \ll t_{\text{adv}}$ the accelerated electrons pile up below the maximum energy γ_{max} given by the equality $t_{\text{rad}} = t_{\text{acc}}$, forming a very flat energy distribution for $\gamma \lesssim \gamma_{\text{max}}$, as illustrated for solar flare conditions by Petrosian & Donaghy (1999). The efficiency and the characteristics of the process in the hotspots are unknown, but the energy density of the electrons, u_e , cannot exceed the energy density of the turbulent magnetic field, u_T .

For hotspots A and D, using parameters derived from radio spectra (Sect. 1) the timescale for particles to escape from the acceleration site considered is $t_{\text{adv}} \sim L/\beta_{\text{out}}c = 3.3 \times 10^4$ yr, where the hotspot size $L \sim 1$ kpc, and we take $\beta_{\text{out}} \approx 0.1$. The radiative (synchrotron) timescale is $t_{\text{rad}} \sim 6\pi m_e c / \sigma_T B^2 \gamma = 2.5 \times 10^9 \gamma^{-1}$ yr with $B \sim 10^{-4}$ G. Thus, for high energy electrons with $\gamma \gtrsim 10^5$, $t_{\text{rad}} < t_{\text{adv}}$, as required for formation of the flat-spectrum high energy electron distribution. For the particle acceleration timescale, we take the ‘optimistic’ estimate (Stawarz & Ostrowski 2002):

$t_{\text{acc}} \sim \zeta^{-1} (c/v_{\text{sc}})^2 (r_e/c) = 2.1 \times 10^{-11} \zeta^{-1} \beta_{\text{sc}}^{-2} \gamma$ yr, where $r_e = \gamma m_e c^2 / e B$ is the electron gyroradius, $v_{\text{sc}} = \beta_{\text{sc}} c$ is a characteristic velocity of the scattering centres (propagating magnetic field inhomogeneities, weak oblique shocks, etc.) and $\zeta = u_T/u_B$ is the ratio of the energy density of the turbulent magnetic field to that of the large-scale mean field. ζ is expected to be less than unity. v_{sc} can be identified with the Alfvén velocity or with the sound speed in the downstream region. The jet plasma is mildly relativistic and so the sound speed in the acceleration region can reach high values $\sim c/\sqrt{3}$, and for approximate equipartition between the downstream particles and the downstream magnetic field, the Alfvén speed is expected to be in the range $\sim 0.1 - 1 c$. Therefore we conservatively take $\beta_{\text{sc}} \sim 0.1$. The maximum electron Lorentz factor and the maximum photon energy of the resulting synchrotron emission are then $\gamma_{\text{max}} \sim 10^{10} \zeta^{1/2} \beta_{\text{sc}}$ and $\varepsilon_{\text{max}} \sim 100 \zeta \beta_{\text{sc}}^2$ MeV, so that for $\zeta = 0.1$ and $\beta_{\text{sc}} = 0.1$, $\gamma_{\text{max}} \sim 3 \times 10^8$ and $\varepsilon_{\text{max}} \sim 100$ keV.

The synchrotron luminosity of the flat electron population can be estimated as $L_{\text{syn}} \sim 10^{38} V \eta \gamma_{\text{max}} \text{ erg s}^{-1}$ (e.g. Stawarz et al. 2004), where V is the volume in kpc^3 and $\eta = u_e/u_B$ is expected to be much less than unity for this electron component. Thus, we conclude that the synchrotron luminosity of this population of high-energy electrons *can be comparable* with the SSC luminosity of the ‘primary’ electrons responsible for the hotspot radio emission.

3 DISCUSSION AND CONCLUSIONS

Our analysis has revealed outer and inner regions of enhanced hardness for the secondary hotspots. The outer hard arcs may constitute a detection of the bow shocks. The inner hard arcs may indicate the sites of the jet terminal shocks and suggest that the jets still interact with the secondary hotspots. We note a similar inner feature in the primary hotspot B, suggesting that the jet is interacting with this hotspot to form a jet terminal shock in the synchrotron lobe formed by earlier jet activity. The absence of an outer arc may be explained by the jet not forming a bow shock until it reaches the intracluster plasma outside the lobe (cf. Stawarz 2004).

As the present data do not allow detailed spectral analysis of the hard features in regions of relatively low X-ray brightness we do not attempt an elaborate physical model,

but consider qualitatively two possible mechanisms. The first is thermal radiation of shocked plasma at the bow shock. In this case, the present results would demonstrate the presence of hot gas in the plasma sheath between the bow shock and the contact discontinuity separating it from the compressed jet non-thermal medium. The free-free radiation of a shocked one-temperature plasma may explain the hardness of the hard outer arcs in hotspot A and D and the temperature estimated for a shock heated region is consistent with values implied by observation although these are not well-constrained. The presence of such plasma could be revealed in high resolution Faraday rotation and/or depolarization maps if observed at frequencies $\nu \lesssim 5\text{GHz}$. However, it is a problem for the thermal model to explain the inner hard arcs because of their apparent location near the jet terminal shocks, where thermal plasma is expected to be absent.

The second process is efficient second-order Fermi acceleration acting non-uniformly within the hotspots. The results would imply a highly perturbed medium in the sheared regions near the contact discontinuity and, possibly, near the jet terminal shock. Thus because it is reasonable to assume the same process forms both inner and outer arcs, and the thermal model cannot explain the inner arcs, we suspect that the hard features discovered in the present work are a manifestation of continuous particle acceleration taking place for the outer arcs close to the contact discontinuity between the downstream jet plasma and the shocked outer gas, and for the inner arcs near the jet terminal shock.

We thank Dr. H. Ebeling for helpful discussions; MO thanks Prof. R. Schlickeiser for his hospitality during a stay in Bochum. This work made use of the *Chandra* data archive and was supported in part by the Polish Committee for Scientific Research by grants PBZ-KBN-054/P03/2001 and KBN-1528/P03/2003/25.

REFERENCES

- Blandford R. D., Rees M. J., 1974, MNRAS, 169, 395
 Brunetti G., Mack K.-H., Prieto M. A., Varano S., 2003, MNRAS, 345, 40
 Carilli C. L., Barthel P. D., 1996, A&A Rev., 7, 1
 Carilli C. L., Perley R. A., Dreher J. W., 1988, ApJ, 334, L73
 Carilli C. L., Perley R. A., Dreher J. W., Leahy J. P., 1991, ApJ, 383, 554
 Carilli C. L., Kurk J. D., van der Werf P. P., Perley R. A., Miley G. K., 1999, AJ, 118, 2581
 Dickey J. M., Lockman F. J., 1990, ARA&A, 28, 215
 de Young D. S., 2002, NewAR, 46, 393
 Dreher J. W., Carilli C. L., Perley R. A., 1987, ApJ, 316, 611
 Hardcastle M. J., Alexander P., Pooley G. G., Riley J. M., 1998, MNRAS, 296, 445
 Hardcastle M. J., Harris D. E., Worrall D. M., Birkinshaw M., 2004, ApJ, accepted (astro-ph/0405516)
 Hargrave P. J., Ryle M., 1974, MNRAS, 166, 305
 Harris D. E., Carilli C. L., Perley R. A., 1994, Nature, 367, 713
 Heavens A. F., Meisenheimer K., 1987, MNRAS, 225, 335
 Kino M., Takahara F., 2004, MNRAS, 349, 336
 Leahy J. P., Perley R. A., 1995, MNRAS, 277, 1097
 Meisenheimer K., 2003, NewAR, 47, 495
 Meisenheimer K., Röser H.-J., Hiltner P. R., Yates M. G., Longair M. S., Chini R., Perley R. A., 1989, A&A, 219, 63
 Meisenheimer K., Yates M. G., Röser H.-J., 1997, A&A, 325, 57
 Mizuta A., Yamada S., Takabe H., 2004, ApJ, 606, 804
 Petrosian V., Donaghy T. Q., 1999, ApJ, 527, 945
 Prieto M. A., Brunetti G., Mack K.-H., 2002, Science, 298, 193
 Sanders J. S., Fabian A. C., 2001, MNRAS, 325, 178
 Röser H.-J., Meisenheimer K., 1987, ApJ, 314, 70
 Scheuer P. A. G., 1974, MNRAS, 166, 513
 Scheuer P. A. G., 1982, In *'Extragalactic radio sources'*, IAU Symp. 97, D. Reidel Publishing Co., p. 163
 Smith D. A., Wilson A. S., Arnaud K. A., Terashima Y., Young A. J., 2002, ApJ, 565, 195
 Stawarz L., 2004, ApJ, accepted (astro-ph/0403179)
 Stawarz L., Ostrowski M., 2002, ApJ, 578, 763
 Stawarz L., Sikora M., Ostrowski M., Begelman M. C., 2004, ApJ, 608, 95
 Williams A. G., Gull S. F., 1985, Nature, 313, 34
 Wilson A. S., Young A. J., Shopbell P. L., 2000, ApJ, 544, 27

This figure "fig1.jpg" is available in "jpg" format from:

<http://arxiv.org/ps/astro-ph/0411502v1>

This figure "fig2a.jpg" is available in "jpg" format from:

<http://arxiv.org/ps/astro-ph/0411502v1>

This figure "fig2b.jpg" is available in "jpg" format from:

<http://arxiv.org/ps/astro-ph/0411502v1>